Subnanosecond Polarized Fluorescence Photobleaching: Rotational Diffusion of Acetylcholine Receptors on Developing Muscle Cells

Yifeng Yuan* and Daniel Axelrod*†
*Biophysics Research Division and †Department of Physics, University of Michigan, Ann Arbor, Michigan 48109 USA

ABSTRACT Polarized fluorescence recovery after photobleaching (PFRAP) is a technique for measuring the rate of rotational motion of biomolecules on living, nondeoxygenated cells with characteristic times previously ranging from milliseconds to many seconds. Although very broad, that time range excludes the possibility of quantitatively observing freely rotating membrane protein monomers that typically should have a characteristic decay time of only several microseconds. This report describes an extension of the PFRAP technique to a much shorter time scale. With this new system, PFRAP experiments can be conducted with sample time as short as 0.4 μs and detection of possible characteristic times of less than 2 μs. The system is tested on rhodamine-α-bungarotoxin-labeled acetylcholine receptors (AChRs) on myotubes grown in primary cultures of embryonic rat muscle, in both endogenously clustered and nonclustered regions of AChR distribution. It is found that ~40% of the AChRs in nonclustered regions undergoes rotational diffusion fast enough to possibly arise from unrestricted monomer Brownian motion. The AChRs in clusters, on the other hand, are almost immobile. The effects of rat embryonic brain extract (which contains AChR aggregating factors) on the myotube AChR were also examined by the fast PFRAP system. Brain extract is known to abolish the presence of endogenous clusters and to induce the formation of new clusters. It is found here that rotational diffusion of AChR in the extract-induced clusters is as slow as that in endogenous clusters on untreated cells but that rotational diffusion in the nonclustered regions of extract-treated myotubes remains rapid.

INTRODUCTION

There are two distinct populations of acetylcholine receptors (AChRs) in living rat myotube plasma membranes: one is clustered, the other is nonclustered. AChRs can form clusters in cell-substrate contact regions (endogenous clusters). Clusters can also be induced by a variety of neural and aneural stimuli, such as rat spinal cord explants (Frank and Fischbach, 1979; Podleski et al., 1978), cell-free nerve extract (Podleski et al., 1978), embryonic brain extracts (Jessell et al., 1979; Salpeter et al., 1982; Olek et al., 1983; Daniels et al., 1990), agrin (a neural protein) (Godfrey et al., 1984; Wallace, 1989; Campanelli et al., 1991; Lupa and Caldwell, 1991; Nastuk and Fallon, 1993), gelasmin (a basal lamina-associated protein) (Barald et al., 1987), polylysine-coated latex beads (Peng et al., 1981), and electric field (Poo and Young, 1990; Stollberg and Fraser, 1988, 1990a). Studies of the mechanism of AChR clustering have been of considerable interest because AChR clustering at neuromuscular junctions is essential for proper signal transduction. Equally interesting is the state of aggregation of AChRs in nonclustered regions, because it can be from nonclustered regions that AChRs are gathered into clusters (Stya and Axelrod, 1983; Anderson and Cohen, 1977).

Studying the rotational mobility of the two distinct populations of AChR in cell plasma membranes may provide some insights into the AChR clustering process. First, rotational diffusion measurements when combined with measurements of lateral diffusion conducted earlier (Axelrod et al., 1976; Axelrod et al., 1978; Cherry, 1979; Edidin, 1987) should provide an understanding of the membrane environment of AChRs on myotubes. In complex biological membranes, rotational and lateral mobilities could be completely decoupled. For example, certain membrane protein molecules might be free to rotate, but lateral motion might be retarded by a tether, anchor, or barrier. On the other hand, free rotation might be inhibited by cross-linking but lateral motion enhanced by nondiffusive actively driven jumps (Velez et al., 1990). Second, rotational diffusion coefficients, which are more sensitive to changes in size and shape of the rotating molecules, can be used to estimate the number of AChRs in an aggregate, if the aggregate is assumed to rotate freely. Third, comparing the dynamic properties of AChRs before and after treatment with AChR aggregating factors may lead to some clues about the mechanisms of the clustering process.

Polarized fluorescence recovery after photobleaching (PFRAP) is a technique for measuring the rate of rotational motion of biomolecules (Velez and Axelrod, 1988; see also Yoshida and Barisas (1986) for a related variation called fluorescence depletion anisotropy). Compared with other existing techniques (such as phosphorescence depolarization; Lo et al., 1980; Bartholdi et al., 1981), this technique has two major advantages: (1) it does not require sample deoxygenation so that it can be applied to living cells under physiological conditions and (2) the characteristic time of the rotational motion of the biomolecules under study can extend over a wide range. In PFRAP, the fluorophore orientations as defined by the directions of the transition dipole

Received for publication 9 January 1995 and in final form 4 May 1995.

Address reprint requests to D. Axelrod, Biophysics Research Division, University of Michigan, 930 N. University, Ann Arbor, MI 48109. Tel.: 313-764-5280; Fax: 313-764-3323; E-mail: daxelrod@umich.edu.

Dr. Yuan's present address: Unilever Research US, 45 River Rd., Edgewater, NJ 07020.

0006-3495/95/08/690/11 $2.00

moment are initially isotropically distributed. An anisotropic orientational distribution is generated by partially bleaching the sample of fluorophores with a brief intense pulse of linearly polarized light. A fluorophore whose dipole moment is oriented to have a larger component along the polarization of the bleaching light will be more likely to be bleached. After bleaching, the anisotropic distribution of fluorophore orientation will relax to isotropicity by rotational diffusion. This relaxation is monitored by a probe beam that is four or more orders of magnitude lower in intensity than that of the bleaching beam and has a linear polarization either parallel to or perpendicular to the polarization of the bleaching beam. The resulting time-dependent postbleach fluorescence recovery reflects the characteristic time of the rotational diffusion of the fluorophores. This PFRAP technique has been used to study rotational diffusion of AChRs on cultured rat myotubes (Velez et al., 1990), chromatin reorientation in intact nuclei (Selvin et al., 1990), DNA reorientation in agarose gels (Scalettar et al., 1990), rotational motion of antibodies and lipids associated with a substrate-supported phospholipid monolayers (Timbs and Thompson, 1990), and myosin head rotation in muscle fibers (Hellen et al., 1993).

The previous PFRAP study of the rotational mobility of AChR found that AChRs in cluster areas were essentially immobile, whereas AChRs in nonclustered areas were a mixture of different fractions rotating at different rates (Velez et al., 1990). The highest rotational diffusion coefficient found was $\sim 700\ s^{-1}$. However, the sample time of that study was limited by instrumentation to $>10\ \mu s$ and the measurable characteristic times to $>\sim 50\ \mu s$. That time scale excludes the possibility of quantitatively observing freely rotating AChR monomers, which should have a characteristic decay time of only $\sim 5\ \mu s$ according to a hydrodynamic theory (Saffman and Delbruck, 1975).

Here we report an extension of the PFRAP technique to a much shorter time scale, with an application to living myotube AChR. We employ a N_2/dye-pulsed laser as a bleaching source (0.5-ns pulse duration) and a fast A-to-D data acquisition interface (Axelrod et al., 1992) that samples at 10-ns intervals. As the duration of the subnanosecond bleaching pulse is shorter than the typical fluorescence lifetime of a few nanoseconds, the bleaching phenomena familiar for conventional PFRAP (with $\sim 100\ \mu s$ or longer bleach duration during which a typical fluorophore goes through several thousand excitations before irreversibly bleaching) are not relevant here. However, it has been demonstrated recently that subnanosecond laser flashes do indeed produce significant bleaching, that both two-photon effects and reversible bleaching are involved, and that polarized bleaching does produce an anisotropic orientational pattern of unbleached fluorophore (Yuan and Axelrod, 1994). With this new system, we were able to conduct PFRAP experiments with a sample time as short as $0.4\ \mu s$ and detection of possible characteristic times of as low as $2\ \mu s$, a 25-fold increase in speed compared with previous PFRAP implementations.

The biological sample used was tetramethyl rhodamine-α-bungarotoxin (RBGT)-labeled AChRs on myotubes grown in primary cultures of embryonic rat muscle, in both clustered and nonclustered regions of AChR distribution. In another additional step from previous work on this biological system (aside from increased speed), we report on the effects of rat embryonic brain extract (containing unidentified and nonquantified AChR aggregating factors) on the fast PFRAP-measured rotational diffusion rates of AChRs.

MATERIALS AND METHODS

RBGT immobilization

The initial postbleach fluorescence anisotropy (as measured by PFRAP) from RBGT-labeled AChRs on the living myotubes is expected to vary from zero for very fast rotation (beyond the speed of our apparatus) to some maximal value for completely immobilized samples. In theory, the maximal value of anisotropy is 4/7 (0.57) (Velez and Axelrod, 1988). However, the actual experimental initial value is always significantly lower than 0.57. This reduction can occur for several possible reasons, among which are that (1) some fraction of the fluorophore may be rotating very rapidly (e.g., as in restricted wobble of the fluorophore around its attachment bond) on a time scale shorter than the experimental sample time; (2) the bleaching anisotropy decreases (in theory) with bleaching light intensity and bleaching depth (Velez and Axelrod, 1988; Hellen and Burghardt, 1994; Yuan, 1994), and (3) the high numerical aperture of a microscope objective leads to some effective depolarization (Axelrod, 1989). To calculate the fraction of AChRs that rotate at measurable speeds, we must know what is the actual maximal anisotrophy as reduced by these effects. We therefore measured anisotropy from RBGT immobilized on coverslips with the same bleaching light intensity and bleaching depth as used in AChR experiments. The anisotropy of this sample is considered the maximal value obtainable from immobilized AChRs.

RBGT (Molecular Probes, Inc., Eugene, OR) was covalently attached to fused silica coverslips (25 mm in diameter) (Esco Products, Oak Ridge, NJ) by using a technique based on one developed by Jacobson et al. (1978) for coupling poly-L-lysine to glass beads and adapted for use in our lab by Fulbright and Axelrod (1993). Fused silica for coverslips was required to avoid the transient luminescence of regular glass, which persists for approximately a millisecond.

Cell cultures

The procedure was previously described by Axelrod et al. (1976). In brief, pregnant rats (strain CD from Charles River Laboratories, Portage, MI) were killed on the 21st day post-coitus by CO_2 asphyxiation. Thigh muscles from the embryos were removed and tweezed apart in Hanks' balanced salt solution (HBSS). The muscle tissue was then digested in 1.5 mg/ml trypsin for 50 min at 37°C in a shaker at 200 shakes per minute. After centrifuging to remove the supernatant containing trypsin, the remaining tissue was transferred to a medium containing 90% Dulbecco's Modified Eagle's medium, 10% fetal calf serum, and 100 μg/ml penicillin/streptomycin. After mixing well, the cell suspension was filtered through two sheets of lens paper. The volume of the medium containing the cell suspension was adjusted to a cell count of 3.5×10^5 cells/ml, and 2-ml aliquots of this cell suspension were added to 35-mm tissue culture dishes each containing a clean and sterile 25-mm diameter fused silica coverslip. The medium was replaced on day 4 with fresh medium that contained 0.6 μg/ml tetrodotoxin. Cells were usually examined on days 6–7 after plating.

Cell cultures were labeled with RBGT just before fluorescence experiments. The medium was removed and washed with HBSS once, then replaced with a solution of fluorescent RBGT at approximately 10^{-7} M in HBSS for ~20–30 minutes at 22°C. After washing twice with HBSS, the coverslip was mounted in a sealed chamber, with the cell surface facing

inside the chamber immersed in HBSS. RBGT binding is irreversible on the time scale of our experiments. For preparing cells for measurement of background fluorescence, the same procedure was followed except that the culture was first exposed to unlabeled α-bungarotoxin at 10^{-7} M for 30 min at 22°C before exposure to RBGT.

Cell culture coverslip treatment

Fused silica coverslips were first immersed in 70% ethanol for at least 30 min and allowed to dry in the air under a sterile hood. Just before plating cells, a solution was made consisting of 0.7 ml of solution A (0.1 ml of HBSS plus 10 ml of 0.1 M NaOH), 0.25 ml of 0.1 M NaOH, 0.25 ml of 0.35 g/100 ml ddH_2O $NaHCO_3$, and 1.6 ml of type I collagen solution from calf skin (Sigma Chemical Co., St. Louis, M.). All solutions were sterile and kept on ice. The coverslips were then coated with the freshly made solution and left in an incubator (37°C, 92% air 8% CO_2, 100% humidity) for 30 min before they were ready for cell plating.

Embryonic brain extract treatment

Embryonic brain extract (EBX) was prepared with a slightly modified version of the procedure described by Jessel et al. (1979). Brain extract was prepared by homogenizing 21-day rat embryo brains with a Dounce homogenizer in 3 vols of Dulbecco's phosphate-buffered saline at 4°C. The homogenate was centrifuged at 1500 *g* for 10 min and the supernatant was centrifuged again at 20,000 *g* for 60 min. The final supernatant contained 3 mg of protein per milliliter as determined by Bradford assay (Bradford, 1976) and was stored at −20°C in small aliquots. The aliquots were thawed only once just before use. The same preparation was used for all experiments. A 100-μl/volume of this brain extract was added to one cell culture dish (2 ml) 24 hours before they were examined for fluorescence.

Optics and electronics for PFRAP

The optical and electronic system for fast PFRAP is shown in Fig. 1. It is a significant upgrade of the previous system (Velez and Axelrod, 1988) in that (1) it is capable of operating at an effective photon-counting sample time down to 0.4 μs, (2) the polarization contrast of the bleaching beams is much improved, and (3) a feedback closed loop in the microscope stage motion system permits automated searching and data acquisition procedures.

This system interchangeably uses either a CW argon laser (Coherent, Inc. Palo Alto, CA; 15W Innova 20, output of 4–6 W at 514 nm) or a nitrogen laser-pumped dye laser (Laser Photonics, Inc. Orlando, FL; output of ~250 μJ/pulse of 0.5 ns tuned at 514 nm) as the bleaching beam source. The CW laser is always the source of the probe beam.

For the case of CW laser bleaching, the horizontally polarized laser beam passes through a long focal length lens L1, through two successive acousto-optic modulators AOM1 (IntraAction, Inc. Bellwood, IL; 40 MHz) and AOM2 (NEC, 140 MHz) activated by the same signal, to reach a focus at a diaphragm D2 that transmits only the first order diffraction beam from the modulators. Two modulators are used in series to ensure a very high (10^6:1) contrast ratio between the on and off states of the bleach beam. The bleach beam continues through a horizontal polarizer prism (P) and a quarter waveplate (QW) to produce circular polarization.

For the case of pulsed laser bleaching, an alternate path is used up to this same point. The unpolarized pulsed laser beam is focused by lens L2 through a circular diaphragm D5, recollimated by lens L3, and joined to the subsequent path of the bleach beam by a variable density beam splitter. The bleach beam is then split by a polarizing cube (PBS1); the horizontally polarized component passes straight through and the vertically polarized component is deflected 90°. The relative intensity of these two polarizations is adjusted by a neutral density filter (NDF). During the dead time between each bleach/recovery cycle, either one of these two orthogonal polarized bleaching beams is alternately selected for the bleach of the next cycle by blocking the other polarization with a solenoid-driven flag under computer control.

The probe beam is always generated by the CW laser, regardless of the source of the bleach beam, and it always has a fixed polarization (horizontal). Before the CW laser beam encounters the AOM, the probe beam path is created by reflection from the surface of a 45° optical flat beam splitter (BS1). The probe path is then recombined with the bleach path at another optical flat beam splitter (BS2) after the latter has passed through the polarization-switching system.

Both the bleach and probe beams pass through a simple converging lens L4 that focuses them onto the field diaphragm plane of an epifluorescence microscope (Leitz Diavert). The beams reflect at a dichroic mirror up through the objective (Zeiss 40× NA = 1.30 oil immersion) and onto the sample. The emitted fluorescence, captured by the same objective and transmitted through the dichroic mirror, passes through a film polarizer that is always oriented to transmit horizontally polarized light.

The fluorescence photons are captured by the single photon counting module (SPCM) (EG&G), which converts each detected photon arrival event into a positive-going square pulse of 2 V and ~200 ns. The SPCM avoids the large transients found to be induced in a standard photomultiplier tube by the discharge spark of the N_2 pulsed laser nearby. The SPCM was also impervious to damage from the bright fluorescent flash during the

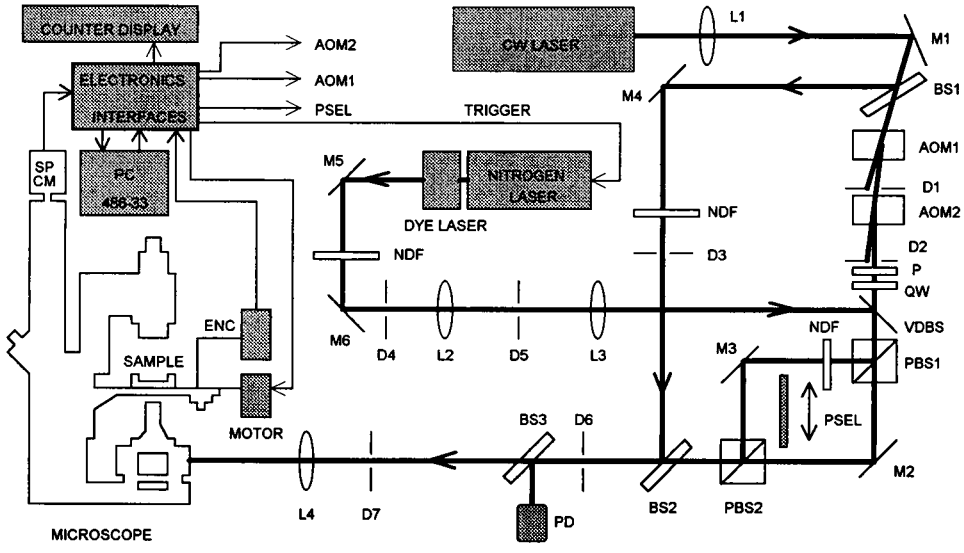

FIGURE 1 Fast PFRAP system optics and electronics. L, lens; M, mirror; D, diaphragm; AOM, acousto-optic module; BS, beam splitter; PBS, polarizing beam splitter; VDBS, variable density beam splitter; P, linear polarizer; QW, quarter-waveplate; PSEL, polarization selector (solenoid-driven flag); NDF, neutral density filter; PD, photodiode; SPCM, single photon counting module (an avalanche photodiode); ENC, linear encoders.

bleaching pulse, unlike a photomultiplier, so no protection circuitry for the detector is necessary.

The photon signal pulse is provided to two different data acquisition boards installed in a 486-based computer, each handling a different time scale range. One board, not used here, is a timer-counter board (CTM-05, MetraByte Corp., Taunton, MA) for sample times of tens of microseconds or longer, custom programmed for photon counting in Fortran/assembly language. However, as we were mainly interested in detecting whether there was any fast rotational diffusion of AChR not detected in the previous slow version of the system, all the PFRAP experiments on cell cultures reported here were done with a different board: a fast A-D converter/memory board (STR-8100, Sonic, Inc., Springfield, VA). The STR-8100 card samples the incoming photon pulse stream as an analog voltage once every 10 ns and then digitizes and stores the results of each bleach/probe cycle (a run) in its on-board 64K memory. The data of the run are then read from the board into the computer memory during the subsequent interval between runs (generally several tenths of seconds). Custom-written software then performs a threshold discrimination and counts the number of greater-than-threshold events in each of a sequence of 0.4-μs time intervals.

Data acquisition

Despite the broad and mixed mode intensity structure of the pulsed laser beam, a series of diaphragms ensured that the final bleaching spot on the sample was nearly circular, with a radius of $\sim$2 μm. NDF were used to adjust the bleaching power to make the bleaching depth $\sim$40% (i.e., 40% of fluorophores were bleached) to avoid the effect of bleaching depth on anisotropy. The actual bleaching intensity delivered to the sample was in the range of 10^{26}–10^{27} photons/cm^2-s. The probe beam was an approximately circular Gaussian with a characteristic radius of less than 0.5 μm. The intensity of the probe beam at its center was $\sim 10^{-5}$ of bleaching beam intensity.

In each run, 200 bins of prebleach and 800 bins of postbleach fluorescence, covering a postbleach recovery of 320 μs, were collected. Signal averaging was essential as there were only 0.06 photons in a bin (0.4-μs sample period) on average for a typical count of 150,000 photons/s. A total of 10,000 runs typically in each polarization gave a total number of 600 photons in a bin, resulting in a statistical uncertainty of fluorescence of $\sim$4%. Note that the uncertainty of anisotropy will be much higher because the anisotropy involves relatively small differences in shape between fluorescence curves taken with orthogonal bleach polarizations (see section on Fitting below).

Stage motion

Two stepper motors (Compumotor Division, Parker Hannifin Corp. Rohnert Park, CA) drive the microscope stage in X and Y directions. The smallest linear distance moved by one motor step is 0.04 μm. The actual stage motion is monitored by two encoders (Heidenhain Corp. Schaumburg, IL), one in each axis. The stage can also be moved manually by a potentiometric joystick (CL Products, Vista, CA). The stepper motors, the encoders, and the joystick all communicate through a motion control card (PC-23, Compumotor).

Each run was done on a fresh spot on the myotube target area; a sequence of such runs was obtained by computer-controlled stage motion and then signal averaged on-line. Before the start of the runs, a polygon enclosing the target area on a myotube, either a cluster or a nonclustered area, was marked out manually by pressing buttons on a joystick stage motion controller to record the coordinates of the polygon's corners. (Clusters with dark spots or nonclustered areas with granular appearance were avoided.) Once the searching and marking were done, the coordinates of all bleaching spots enclosed by the polygon were computed by the PC (step size was 5 μm to avoid overlapping on partially bleached areas) in a raster array. To minimize the effect of biological variation over large distances on the myotube surface, the bleaching beam was automatically alternated between parallel and perpendicular polarization at the immediately adjacent bleaching spots by flipping a solenoid-driven flag blocking one beam or the other.

The whole system is run from the PC by an integrated program through a combination of Fortran, C, and assembly language subroutines for synchronous control of the pulsed laser triggering, polarization selection solenoid, and programmed motorized stage motion and for data acquisition, averaging, display, and recording to disk.

Data corrections

In PFRAP theory, the relative intensities of the parallel and perpendicular bleach pulses are assumed to be equal. If they are not in fact equal, then the sample data must be corrected for the difference. The relative intensities were measured by performing comparable PFRAP experiments on samples that exhibited rapid molecular tumbling on the time scale of the myotube experiments, i.e., an aqueous solution of RBGT sandwiched between fused silica coverslips. In such samples, equal bleach intensities in the two polarizations should give rise to zero anisotropy over the entire time range of our experiments. Conversely, corrections for nonequal bleach intensities can be calculated, if necessary, from a nonzero anisotropy measured on such a sample.

The cell's autofluorescence contribution was determined by gathering PFRAP data on myotubes whose AChR had been blocked by an excess of unlabeled α-bungarotoxin before exposure to RBGT. This background data was subtracted from the PFRAP data taken on RBGT-labeled myotubes.

The SPCM detector has a rather long deadtime; two photons arriving less than 200 ns apart are reported as one output pulse. Therefore, the probe intensity was adjusted (with NDF) to limit the fluorescence photon count rate to under 200,000 counts/s. In addition, a count correction was done after data acquisition, as follows. If x photons are recorded by the SPCM, the real number of photons can be shown to be

$$y = -\frac{t_s}{t_d}\ln\left(1 - \frac{t_d}{t_s}x\right), \tag{1}$$

where t_d = 200 ns is the SPCM deadtime and t_s = 0.4 μs is sample time.

Also in PFRAP theory (as discussed in the next subsection), an emission polarizer is assumed to be present, to circumvent unpredictable partial polarization bias arising from internal mirrors and filters of the particular microscopes employed. However, in these experiments, the emission polarizer reduced the fluorescence counts in nonclustered AChR areas (typically approximately one-eighth as bright as cluster area) to a very low level. To avoid this problem, we measured the bleaching anisotropy of a standard sample (RBGT immobilized on a fused silica coverslip) with and without the emission polarizer. The ratio of the anisotropy with polarizer over the anisotropy without polarizer was found to be 1.6. The emission polarizer thereby was removed for all experiments, and all anisotropies obtained thereafter were multiplied by 1.6.

Fitting

The raw data is the intensity of the prebleach ($t < 0$) fluorescence $F_{\parallel,\perp}(-)$ and the postbleach ($t > 0$) fluorescence $F_{\parallel,\perp}(t)$ for each bleaching polarization $\parallel$ and $\perp$. The bleaching anisotropy is defined by

$$r_b(t) = \frac{\Delta F_\parallel(t) - \Delta F_\perp(t)}{\Delta F_\parallel(t) + 2\Delta F_\perp(t)}, \tag{2}$$

where

$$\Delta F_{\parallel,\perp}(t) = F_{\parallel,\perp}(-) - F_{\parallel,\perp}(t) \tag{3}$$

In principle, the ratio $r_b(t)$ cancels out the effects of reversible bleaching recovery, leaving a time-dependent variable that is independent of the state of sample aerobicity and excited state lifetimes and that preserves the dependence on rotational diffusion. For rotational diffusion in two dimen-

sions about a normal to the membrane plane, such as AChR on a myotube surface, the fluorescence differentials were given by Velez and Axelrod (1988):

$$\Delta F_{\perp}(t) = a - be^{-4Dt} - ce^{-16Dt}$$
$$\Delta F_{\parallel}(t) = a + be^{-4Dt} - ce^{-16Dt}, \quad (4)$$

which leads to

$$r_b(t) = \frac{2be^{-4Dt}}{3a - be^{-4Dt} - 3ce^{-16Dt}}, \quad (5)$$

where D is the rotational diffusion coefficient of the rotating molecules. Factors a, b, and c are complicated functions of the wobble angles of the fluorophore, the angle between the absorption and emission dipoles, and the bleaching depth. Two modifications of Eq. 5 are employed before fitting data, as follows.

First, we approximate $r_b(t)$ in Eq. 5 as a single exponential for a single D, as previously done by Velez et al. (1990). This is reasonable because Eq. 5 can be expanded as a linear combination of exponentials, but the relative magnitudes of a, b, and c at the bleaching depths used here ensure that the higher order terms will have an amplitude of no more than 16% of the first term. Given the considerable noise in the data as a result of photon statistics, this 16% inaccuracy in the approximation is not a significant concern. We are left with an approximately single exponential of decay rate $4D$ for our model of a rotating cylinder about an axis normal to the membrane; this is the leading term in $r_b(t)$ regardless of the amplitude of any fast fluorophore wobbling superimposed on the rotating cylinder motion. (For a full three-dimensional rotational diffusion of the molecule, the decay rate would be $6D$.)

Second, we assume a heterogeneity of rotational rates in the sample, described by two rotational diffusion coefficients D_1 and D_2. The final expression of $r_b(t)$ then becomes

$$r_b(t) = \frac{2b}{3a}[\alpha e^{-4D_1t} + (1 - \alpha)e^{-4D_2t}], \quad (6)$$

where α is the fraction of fluorophores with rotational diffusion coefficient D_1.

If no emission polarizer is used (as done here), then the numerical factors multiplying the exponentials in both the numerator and the denominator of Eq. 5 are somewhat altered. But to the accuracy of the single exponential approximation used here, the multiplication of experimental $r_b(t)$ by an empirically determined factor of 1.6 to correct for the absence of an emission polarization filter (as discussed in the previous section) is valid.

All nonlinear fitting procedures were performed with the microsoft Windows-based graphics program Origin (MicroCal Software, Inc., Northampton, MA). The purpose of fitting is to derive the rotational diffusion coefficients $D_{1,2}$ and fraction α from $r_b(t)$ from noisy data. The uncertainty of $F_{\parallel,\perp}(t)$ comes from photon shot noise that follows a Poisson distribution. However, the probability density of $r_b(t)$ does not follow either a Poisson distribution or a Gaussian distribution because it is formed from a ratio (Eq. 2) involving the $F_{\parallel,\perp}(t)$ values. (To see this clearly, note that a random occurrence of zero in the denominator at some t will lead to an infinity in $r_b(t)$). Therefore it is mathematically unsound to fit the experimental $r_b(t)$ data with the standard nonlinear least-squares methods. We circumvent this problem by the following steps:

(1) To generate a smooth curve that accurately follows the raw fluorescence data $F_{\parallel,\perp}$, we fit the experimental $F_{\parallel,\perp}(t)$ data with four-exponential decay

$$\hat{F}_{\parallel,\perp}(t) = a_1e^{-a_2t} + a_3e^{-a_4t} + a_5e^{-a_6t} + a_7e^{-a_8t} + a_9, \quad (7)$$

with all a_i parameters floating freely with a standard nonlinear least-squares method. Note that the a_i parameters in the exponents are not solely due to rotational diffusion rates, because a large portion of the fluorescence recovery is due to reversible photobleaching. As we do not know an appropriate theoretical shape for the possibly complex reversible photobleaching effect, the experimental $F_{\parallel,\perp}$ is fit with the entirely empirical shape of Eq. 7. Other techniques of smoothing, (e.g., finding best fits to polynomials on successive sequences of data points) are possibly less desirable here because they can suppress the fastest varying components and they can produce artifactual inflection points in the recoveries.

The fitting is performed with a standard weighting based on the uncertainty $\delta F_{\parallel,\perp}$:

$$\delta F_{\parallel,\perp} = \sqrt{F_{\parallel,\perp}/N}. \quad (8)$$

N is the number of runs for each polarization.

(2) An $\hat{r}_b(t)$ is calculated using the fit curves $\hat{F}_{\parallel,\perp}(t)$ according to Eq. 2. This $\hat{r}_b(t)$ is essentially a smooth representation of the non-Gaussian noisy $r_b(t)$ that could have been computed directly from the raw fluorescence data.

(3) The uncertainty $\delta\hat{r}_b(t)$ arises from the theoretical Poisson shot noise of the fluorescence as represented by the fit values $\hat{F}_{\parallel,\perp}(t)$ and is calculated for each bin by standard error propagation (Bevington and Robinson, 1992):

$$\delta\hat{r}_b = \frac{(3/\sqrt{N})\sqrt{(\hat{F}_0 - \hat{F}_{\perp})^2\hat{F}_{\parallel} + (\hat{F}_0 - \hat{F}_{\parallel})^2\hat{F}_{\perp}}}{[3\hat{F}_0 - (\hat{F}_{\parallel} + 2\hat{F}_{\perp})]^2}. \quad (9)$$

For our experiments, the relative uncertainty of anisotropy $\delta\hat{r}_b/\hat{r}_b$ is many times higher than the relative uncertainty of fluorescence $\delta F_{\parallel,\perp}/F_{\parallel,\perp}$, as r_b depends on the rather small difference between two already noisy quantities, $F_{\parallel}$ and $F_{\perp}$. For our data, the relative uncertainty of anisotropy is ~20–25% at initial postbleach recovery, and ~70–85% near the end of the recovery (320 μs).

(4) We then fit the calculated $\hat{r}_b(t)$ with a double exponential decay, using the uncertainty $\delta\hat{r}_b(t)$ to determine the weighting in a standard nonlinear least-squares method. The fitted rates and amplitudes are then related to rotational diffusion coefficients and mobile fractions according to Eq. 6. As no constant parameter is added to the double exponential, any "immobile" fraction is folded into the slower rotating fraction.

Two simulations described in the Appendix were conducted to demonstrate that (1) the systematic fitting procedure does extract information about the rotational mobility of fluorophore sample and (2) it does not introduce artifacts such as a false fast rotational component.

The fitting procedure was first performed on uncompressed data (sample bin 0.4 μs). The result was that the fastest decay component detected had a characteristic time of ~20–30 μs. This suggested that we could safely compress raw data fourfold to sample bin 1.6 μs (which is less than one-tenth of the shortest decay time found by the fitting procedure) to increase the signal/noise ratio. Fitting in both uncompressed and compressed raw data yielded the same results.

RESULTS

Immobile and rapidly mobile RBGT

The sample of rapidly mobile RBGT was made by dissolving RBGT in HBSS at ~10^{-7} M. The solution was sandwiched between two fused silica coverslips. The very short rotational correlation time of this sample (~5 ns) guaranteed that no anisotropy generated by a bleaching light pulse would be retained in the time scale of our PFRAP (sample time = 0.4 μs). This characteristic made it an excellent control to ensure that the bleaching intensities of the parallel and perpendicular polarizations were the same on the sample and all beams ($I_{\parallel}$, $I_{\perp}$, I_{probe}) were properly aligned. This control was performed on every day of the experiment. Fig.

2 shows that anisotropy of the control sample was indeed at constant zero over the postbleach recovery of 320 μs.

The immobilized RBGT sample was made by covalently attaching RBGT to a fused silica coverslip as described in Materials and Methods. Although the BGT is immobilized in such a preparation, the rhodamine fluorophore is still partially free to wobble on its covalent attachment bond. The resulting bleaching anisotropy is then the upper limit for anisotropy from any RBGT-AChR sample. Any reduction from that maximal value can be attributed to rotational motion of the whole RBGT (and presumably the whole RBGT/AChR complex). Fig. 2 shows that the immobilized RBGT sample had a constant anisotropy of 0.20. This is almost double the value obtained previously (Velez et al., 1990), probably due to the much improved purity of bleaching beam polarization here.

Clustered and nonclustered AChR

Fig. 3 *a* is a photograph of typical endogenous clusters on myotubes labeled with RBGT. Endogenous clusters have an elongated elliptical shape with a typical size of ~40 μm × 15 μm. The regions between clusters also contain AChRs at a fairly uniform but much lower surface concentration; these are the nonclustered regions.

Fig. 4, *a* and *c*, show the fluorescence recovery curves $F_{\|,\perp}(t)$ for clustered and nonclustered regions, respectively, along with the smooth (four-exponential) fits derived for them. Fig. 4, *b* and *d*, shows the bleaching anisotropies $r_b(t)$ calculated directly from that data and also the fits of anisotropies from which diffusion coefficients are obtained.

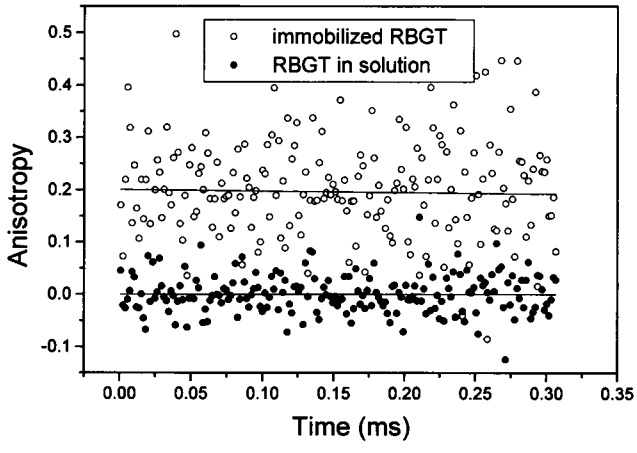

FIGURE 2 Anisotropies of the most immobilized sample (RBGT immobilized on fused silica coverslips) and the most mobile sample (RBGT in HBSS solution). Discrete points are experimental data displayed with 1:4 compression so that each point represents 1.6 μs. Solid and dashed lines are single exponential decay best fits to the uncompressed data for the solubilized and immobilized RBGT, respectively. The solution control (solid circles) has constant zero anisotropy. The immobilized sample (open circles) has nearly constant anisotropy of ~0.20. Bleaching duration = 0.5 ns; bleaching depth ~40%; and sample time = 0.4 μs. Each polarization has ~20,000 runs for the solution control and 12,000 runs for the immobilized sample.

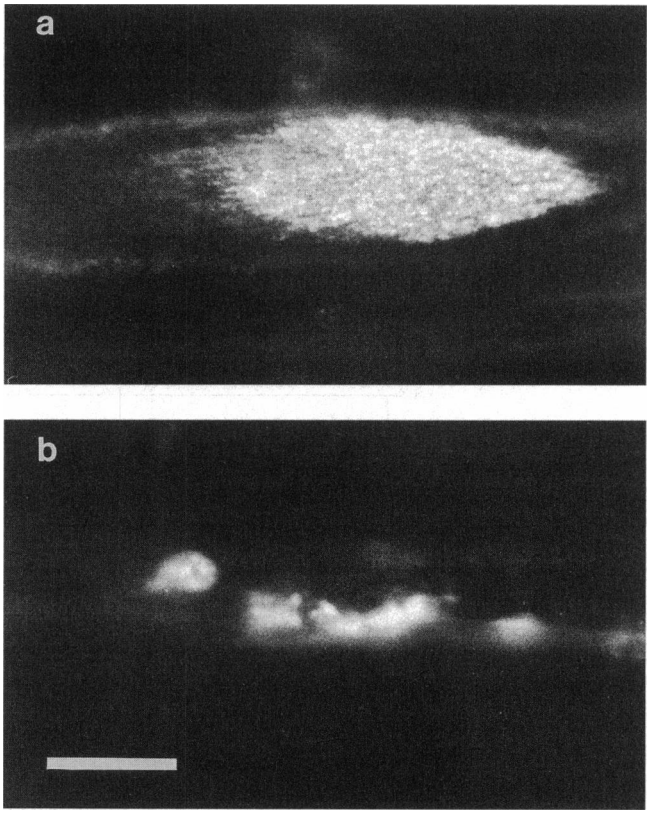

FIGURE 3 Film photographs of myotubes in a rat primary cell culture. (*a*) Without EBX treatment, showing a large endogenous cluster. (*b*) With EBX treatment, showing small and irregularly shaped EBX-induced clusters. Myotubes are approximately 400 μm long and range in width from 15 to 40 μm. For *a*, the focus is at the bottom surface of the myotubes (proximal to the substrate) where the endogenous clusters were located. For *b*, the focus is at the top surface where the EBX-induced clusters were located. The excitation illumination was provided by a defocused 514-nm argon laser beam. Exposure was ~30 s on Kodak P3200 film. Space bar, 20 μm.

The difference between clustered and nonclustered regions is clear; the clustered AChRs have a higher and essentially constant anisotropy indicating a large fraction of rotational immobility in the microsecond to millisecond time range, whereas the nonclustered AChRs show a heterogeneous mixture of components with different rotational rates. These same qualitative features were measured previously in a slower (by almost two orders of magnitude) time scale (Velez et al., 1990). The heterogeneity is reported as an average fast rate and an average slow rate, the latter including in possible part any portion of the AChR that are essentially immobile.

For clusters, $r_b = 0.15 \pm 0.01$. This is smaller than $r_b = 0.20$ found for immobilized RBGT on coverslips. For nonclustered areas, the initial postbleach anisotropy was even lower; $r_b = 0.11 \pm 0.01$. The rotational diffusion coefficients resulting from this data are summarized in Table 1.

Embryonic brain extract treatment

Treatment with EBX disperses old endogenous AChR clusters and triggers new AChR cluster formation on myotubes

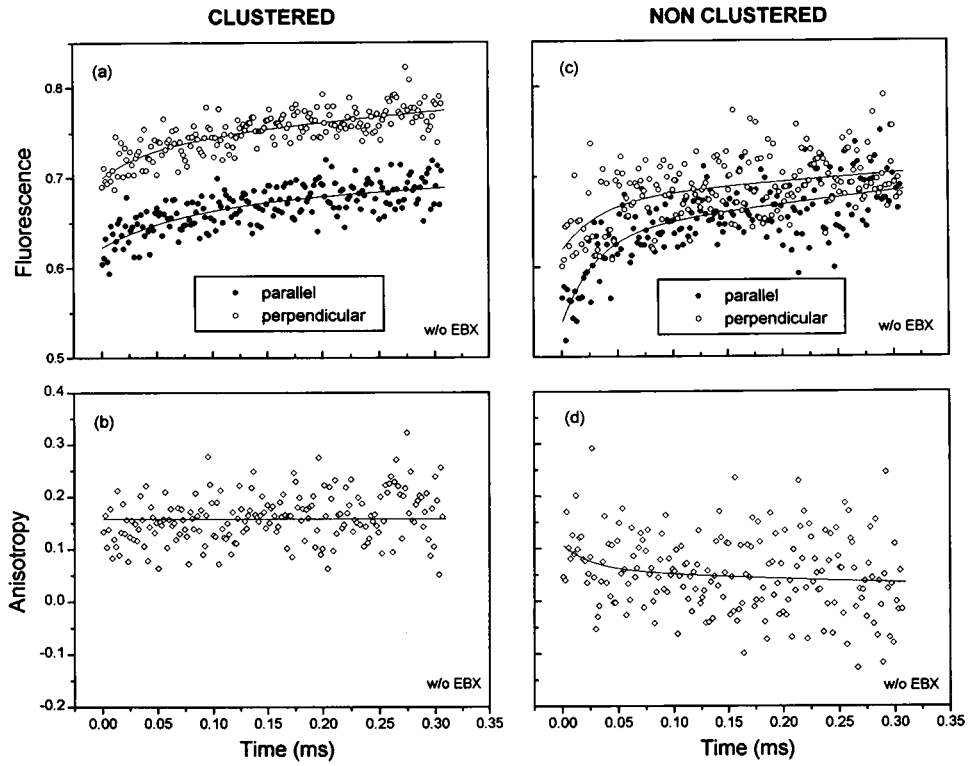

FIGURE 4 (*a*) and (*c*) Fluorescence recovery curves $F_{\parallel}(t)$ (●) and $F_{\perp}(t)$ (○) (as corrected for photon pulse overlap) for clustered (*a*) and nonclustered (*c*) AChR on myotube surfaces of rat primary cultures without EBX treatment. The ordinate scale is normalized to set the average of prebleach points (not shown) to unity. Discrete points are experimental data displayed with 1:4 compression so that each point represents 1.6 μs. Solid lines are four-exponential decay best fits to the uncompressed data; these fits are used subsequently to calculate smooth anisotropy curves. (*b*) and (*d*) Corresponding bleaching anisotropies $r_b(t)$ for clustered AChR (*b*) and nonclustered AChR (*d*) as derived from the fluorescence curves of *a* and *c*, respectively. Solid lines are double exponential decay best fits to the smooth bleaching anisotropy curves formed from the four-exponential fits shown in Fig. 4. Bleaching duration = 0.5 ns; bleaching depth = ~40%; and original sample time = 0.4 μs. Number of runs in each polarization was ~10,000 for nonclustered areas and ~4500 for clusters.

of rat and chick cell cultures (Podleski et al., 1978). The rat muscle cell culture shown in Fig. 3 *b* was from the same preparation and viewed at the same time as that for Fig. 3 *a*, except that rat EBX was added 24 hours before the examination. Almost no endogenous clusters can be seen. Instead, new EBX-induced clusters appear on the top surfaces of myotubes; they are more speckly, smaller, more irregular, and brighter than endogenous clusters.

For EBX-induced speckles, the initial anisotropy r_b = 0.13 ± 0.01, and it is essentially nondecaying. This is lower than the anisotropy from the immobilized RBGT sample and essentially equal (to within the uncertainty) to the anisotropy found in endogenous clusters.

TABLE 1 Rotational diffusion components of AChR in nonclustered areas

	Component	D (s^{-1})	Fraction (%)
Without EBX	Fast	9,600 ± 4,000	44 ± 9
	Slow	440 ± 160	56 ± 8
With EBX	Fast	15,000 ± 10,000	35 ± 12
	Slow	<450	65 ± 6

For nonclustered AChRs on EBX-treated myotubes, the initial anisotropy is 0.09 ± 0.02 and it subsequently decays. Fitting leads to rotational diffusion coefficients as summarized in Table 1. Because the RBGT fluorescence of nonclustered regions on EBX-treated cells is even dimmer than the corresponding regions on untreated cells, the fluorescence and anisotropy data is very noisy and the fitted values thereby have very large uncertainties. A fast rotational diffusion component exists, with a rate and amplitude that overlaps those for nontreated myotubes. A slow rotational component also exists with a substantial amplitude comparable with that measured on nontreated myotubes.

DISCUSSION

AChR rotational diffusion

The two distinct populations of AChR on myotube surface membranes, clustered and nonclustered, are also distinct in their rotational diffusion behavior; most clustered AChRs are rotationally immobile whereas most nonclustered AChR are rotationally mobile. This distinction was demonstrated previously in longer time scale PFRAP experiments, with

sample times varying from 10 μs to 1.5 ms and postbleach fluorescence recovery durations up to 225 ms (Velez et al., 1990), and here in short time scale PFRAP experiments presented (sample time 0.4 μs, postbleach fluorescence recovery duration of 320 μs).

Our measurements in the nonclustered areas showed there are at least two components with different rotational diffusion rates, with the fastest rate not previously measurable. The rotational diffusion coefficient D for the fast component $\sim 10^4$ s^{-1}, whereas D for the slow component is on the order of a few hundreds per second. Velez et al. (1990) found at least three different rotational diffusion rates for nonclustered AChR in the long time scale PFRAP: D = 700, 2.9, and <0.1 s^{-1}, with fractions 15 ± 7, 30 ± 11, and 24 ± 9%, respectively. It appears that our slow component (in our shorter time scale) is a mixture of these components.

Interpretation of diffusional components

Assuming that the slowdown of rotational diffusion is due to more than one AChR monomer forming small aggregates, we can estimate the possible number of monomers in one such aggregate with the following equation (Saffman and Delbruck, 1975):

$$D = \frac{kT}{4V\eta}, \tag{10}$$

where an oligomer is modeled as a cylinder rotating freely about its vertical axis in the two-dimensional viscosic membrane. D is the rotational diffusion coefficient, k the Boltzmann constant, T the temperature, V the volume of the rotating protein oligomer, and η the viscosity coefficient of the membrane. η is typically 1 poise = 0.1 N s/m^2 in membranes. The thickness of the membrane is 7 nm.

For the slow component of AChR rotational motion (D = 440 s^{-1}), Eq. 10 gives the cross-sectional area of the cylindrical aggregate to be 0.03 μm^2. As the packing area per monomer in a close-packed two-dimensional AChR array is $\sim$70 nm^2 (Brisson and Unwin, 1985), an aggregate of 0.03-μm^2 size would be composed of $\sim$400 monomers. However, 400 is an upper limit, because the slowdown of rotational diffusion could be caused by anchoring, a locally high lipid viscosity, or a steric hindrance with other obstacles in the membrane, rather than size alone.

For the previously undetected fast component (D = 9600 ± 4000 s^{-1}), Eq. 10 gives a cross-sectional area of 1.5 × 10^{-4} μm^2, which is only 4–5 times the cross section of an isolated AChR monomer (33 μm^2), indicating that this faster component arises from an oligomer consisting of only a few AChR monomers, and possibly from a single monomeric AChR. The evidence that nonclustered AChRs may be freely diffusing as a monomer or only small microaggregates is new, obtainable because of the extended time range of fast PFRAP.

Embryonic brain extract treatment

EBX has been demonstrated to cause the redistribution of AChRs on the surface of cultured myotubes (Jessell et al., 1979; Salpeter et al., 1982; Olek et al., 1983; Daniels et al., 1990). Similar effects on cloned muscle cells were observed by the addition of spinal cord explants and cell-free nerve extract (Podleski et al., 1978). More specifically, these effects are (1) the increase of the number of AChRs over the entire myotube surface membranes, (2) the dispersion of endogenous clusters at substrate-associated surfaces on myotubes, and (3) the formation of new speckle-like aggregates on the top surface of myotubes. These effects could be seen as early as 4 h after continuous application of EBX.

Our results show that there is no dramatic change in rotational diffusion rates of AChRs in nonclustered area on myotubes of rat primary cultures after addition of rat EBX, although the dim fluorescence here leads to a large uncertainty band. This rough constancy of AChR fast diffusion is unexpected because of the dramatic effect of brain extract in aggregating AChRs, evidently it does not affect all AChRs on the cell surface. Our results also show that the rotational mobility of the EBX-induced clusters is not significantly different from that of the endogenous clusters; both are essentially immobile. This result is also perhaps unexpected, as the EBX-induced clusters, better termed as speckles, bear little resemblance to the endogenous clusters in shape, size, and localization.

The primary active component in EBX responsible for the overall increase of the AChR on the myotube surface membranes was identified as ascorbic acid (Knaack et al., 1987), the function of which is probably to promote synthesis of AChR in skeletal muscle. Although commercial ascorbic acid does cause similar increases of total numbers of AChRs on myotube surfaces, it does not cause significant AChR clustering. It has been suggested by several authors that the AChR clustering effect of EBX is due to another factor or factors of apparent high molecular weight (Neugebauer et al., 1985; Falls et al., 1990; Reist et al., 1992).

The AChR density in EBX-induced aggregates has been found to approach those at the neuromuscular junction (>10,000 sites/μm^2), whereas the AChR site concentration on primary rat muscle cell cultures usually does not exceed 3000–5000 sites/μm^2 (Salpeter et al., 1982). Whereas the endogenous clusters reside at the substrate contact regions of the bottom surfaces of myotubes, the EBX-induced clusters are often associated with membrane bulges on the top surfaces of myotubes. In EBX-treated muscle cells, there is an overall increase in both dense membrane and basal lamina at the top surfaces of the cells and within clusters paralleling the increase in AChR and AChR clusters. Daniels et al. (1990) proposed that AChR aggregates in different systems (clusters in neuromuscular junctions, endogenous clusters, EBX-induced clusters, and clusters induced by other stimuli) were made by a similar mechanism and organized in similar ways, based on the observations that these clusters tended to be enriched in the same cy-

toskeletal proteins, such as vinculin, α-actinin, filamin, actin, 58K protein, and 43K protein (Daniels et al., 1990; Daniels, 1990; Bloch et al., 1989; Rochlin and Peng, 1989; Wallace, 1989; Shadiack and Nitkin, 1991). Our anisotropy results in endogenous and EBX-induced clusters are not inconsistent with their proposal. Our AChR anisotropy results in nonclustered areas with and without EBX treatment suggest that the local environment of the AChR in the nonclustered areas is likely not significantly altered by the addition of EBX.

Low initial anisotropies

The initial anisotropies of AChRs in both clusters and nonclustered areas are lower than the anisotropy of immobilized RBGT on coverslips. Furthermore, that immobilized control sample has an anisotropy value (0.20) that itself is much lower than the theoretical maximum of 0.57 (Velez and Axelrod, 1988). We also find that the initial anisotropy decreases further when bleaching depth increases (Yuan, 1994).

It is unlikely that the low initial anisotropy is due to rotations of the labeled RBGT/AChR complex as a whole. For this to be the case, rotational motions in the RBGT-labeled AChR would have characteristic decay times smaller than the time resolution of our experimental system, which is 0.8 μs (twice the sample time of 0.4 μs), corresponding to a D of 3×10^5 s^{-1}. Such a D is much larger than would be expected for an AChR monomer rotating freely in the membrane.

There are several other causes of a reduction of initial anisotropy. Two of them are inherent in the PFRAP technique itself. Under our experimental conditions, both of these causes of low anisotropy necessarily do occur. The first is the depletion of ground state fluorophore due to the bleaching that is irreversible on the time scale of the bleaching pulse (called irreversible ground state depletion here) (Velez and Axelrod, 1988). Irreversible ground state depletion can be predicted to decrease the initial anisotropy from the theoretical maximal value of 0.57 to 0.51. The second is the saturation of fluorophore excitation during the bleaching pulse (Hellen and Burghardt, 1994). Fluorophore excitation saturation reduces the initial anisotropy further to 0.30.

Another cause of low initial anisotropy value, to which we attribute the decrease from 0.30 to the experimentally measured value of 0.20 on immobilized RBGT on coverslips, is fast wobbling of the rhodamine fluorophore around its attachment bond to the BGT protein (Velez and Axelrod, 1988; Yuan, 1994). The even lower initial anisotropy of the rhodamine on the BGT/AChR/myotube may arise from a wobble that is even faster and/or through a wider angle than rhodamine bound to a BGT/coverslip, due to differences in the local environment. The initial anisotropy of nonclustered area AChRs is even lower than the anisotropy of cluster area AChRs, possibly also because of a different level of fluorophore wobble. According to the theory of PFRAP, very rapid wobble, on a time scale much shorter than the minimal sample time, affects only the initial anisotropy but not the shape of the subsequent bleaching anisotropy decay from which quantitative diffusion coefficients are obtained.

Two more possible phenomena can lead to low anisotropy: energy transfer and quenching among rhodamine groups in close proximity, which tend to reduce fluorescence polarization; and the high numerical aperture of the objective, which tends to mix polarizations (Axelrod, 1989). Again, these phenomena would not affect the time course observed with bleaching anisotropy decay.

The PFRAP technique

Although other techniques have been used to measure rotational motion of the AChR, such as electron spin resonance spectrum (Rousselet et al., 1982) and phosphorescence depolarization (Lo et al., 1980; Bartholdi et al., 1981), deoxygenated membrane fragment preparations of purified *Torpedo* electric organ were used in nonmicroscopic studies. Those experiments showed that the AChRs were virtually immobile in *Torpedo* membranes. Our PFRAP results for rotational mobility of the AChR on cultured myotubes are the first microscopic measurements on living, nondeoxygenated single cultured cells with submicrosecond sample times. These times are significantly shorter than the theoretical characteristic rotational diffusion time of AChR monomers on living cell membranes. In contrast to the immobility previously seen in *Torpedo*, the results presented here demonstrate that the AChR in the nonclustered areas of the living myotube surfaces can rotate with a rotational diffusion coefficient as large as 9600/s. This rapid rate suggests that some nonclustered region AChRs exist in very small aggregates of only a few monomers, and possibly in single monomers, as they rotate freely in the membrane. Our clustered AChR results, which demonstrate predominant immobility, are perhaps analogous to the previous *Torpedo* results.

The related technique of polarized fluorescence depletion (PFD) has also been recently applied successfully to the study of labeled protein rotation on single living cells (Rahman et al., 1992). PFD uses eosin probes in deoxygenated systems. As a result, the fast end of the range of PFD (limited by shot noise) is in principle similar to that for PFRAP, but the slow end for PFD is the decay time of the triplet state (milliseconds) whereas the slow end for PFRAP is essentially infinite.

This study has significantly improved the PFRAP technique in the following aspects. First, the time resolution has been shortened to approximately a microsecond by utilizing a subnanosecond bleaching light source and a fast data acquisition interface. Second, the polarization contrast ratios of the bleaching beams are enhanced such that the measured initial bleaching anisotropy nearly doubles. The higher initial bleaching anisotropy, combined with the available fluorophore with high quantum efficiency and

proper bleachability, makes the PFRAP more feasible for studying biomolecular rotational motion with characteristic times over the entire range from approximately a microsecond to a few seconds. Third, the microscope stage motion control has been completely automated so that PFRAP can be performed feasibly on irregular sample regions on living cell membranes with a typical size of approximately a few micrometers.

Statistical uncertainty due to photon shot noise is clearly the limiting factor in determining the minimal time scale to which PFRAP can be applied. The conditions of these experiments, the very dim samples (especially AChRs in nonclustered areas, which contain only ~1000 fluorophores/μm^2) and the short sample bin times, clearly push the technique to its fast limit. But the rather elaborate curve-fitting procedures used here, designed to handle the high level of non-Gaussian noise in the bleaching anisotropy at the shortest feasible time scale, seems to successfully recover correct diffusion coefficients, as is confirmed in an analysis of artificial data generated with an equivalent noise level (see Appendix).

APPENDIX

A central finding in this project is the presence of a fast component of AChR rotation that is consistent with the presence of free AChR monomers in the membrane in nonclustered regions. But the original data, and particularly the bleaching anisotropy *versus* time curves are very noisy. Therefore, we employ two simulations described below to verify the validity of our fitting procedure. Simulation A shows that the fitting procedure does extract approximately correct information about the rotational mobility of the fluorophore sample despite the presence of a large amount of statistical noise in the data. Simulation B shows that the fitting procedure does not incorrectly report the presence of fast rotational components that do not exist. The starting functions (such as fluorescence recovery and anisotropy) constructed for the simulations were generated to be similar to the real experimental data in shape, time scale, and noise level.

Simulation A: test for correct retrieval of diffusion coefficients

This simulation begins with artificial fluorescence recovery curves $F_{\parallel,\perp}(t)$ generated from the following equation:

$$F_{\parallel,\perp}(t)/F(0) = 1 - \Delta F_{\parallel,\perp}(t)$$
$$= 1 - \alpha(t)(a \pm b_1 e^{-4D_1 t} \pm b_2 e^{-4D_2 t}), \quad \text{(A1)}$$

where the expression in parentheses represents the fluorescence recovery due to rotational diffusion of fluorophores (Eq. 4) and $\alpha(t)$ represents the fraction of bleached fluorophore that remains bleached after time t, reflecting the effect of possible reversible bleaching. To generate curves that closely match the amplitudes, bleaching depths, irreversible bleaching fractions, recovery shapes, anisotropies, and diffusion coefficients corresponding to the experiments, we choose the following parameters prebleach fluorescence $F(0) = 0.04$, $a = 0.35$, $b_1 = 0.02$, $b_2 = 0.03$ (which give relative amplitudes for the fast and slow components of 40 and 60%, respectively), $D_1 = 9600\ s^{-1}$, and $D_2 = 440\ s^{-1}$. For the reversible recovery factor, we set

$$\alpha(t) = k_5 + k_1 e^{-k_2 t} + k_3 e^{-k_4 t}, \quad \text{(A2)}$$

where $k_1 = 0.4071\ s^{-1}$, $k_2 = 40{,}000\ s^{-1}$, $k_3 = 0.3071$, $k_4 = 1000\ s^{-1}$, and $k_5 = 0.2857$.

A noise of 5% (produced by random number generation) is then added to the curves to make the simulated experimental curves for fluorescence recovery. Finally, the same fitting procedure as used in experimental data analysis is applied to the simulated curves.

The fitting procedure reproducibly retrieves diffusion coefficients and relative amplitude fractions, both with calculated uncertainties, of the following values: $D_1 = 12{,}100 \pm 1{,}900\ s^{-1}$, with amplitude fraction of $60 \pm 5\%$; and $D_2 = 180 \pm 370\ s^{-1}$, with amplitude fraction of $40 \pm 3\%$. The fast rate is within 30% and the amplitude is within 50% of the rate and amplitude ($9600\ s^{-1}$ and 40%) with which we started. The existence of a slow rate as indicated by its substantial amplitude fraction is well predicted at a value 33% smaller than the input value. The rate of the slow component returned by the fitting procedure is somewhat uncertain but covers a range restricted to $D_2 < 550\ s^{-1}$, which is consistent with the input value of $440\ s^{-1}$. If the fitting procedure is repeated on simulated data sets with different random numbers (but the same variance), the returned values generally range within 15% of the ones quoted here. We can therefore conclude that, despite the large amount of noise, the fitting procedure clearly retrieves reasonable approximations to the known input values.

Simulation B: test for artifactual fast components

In this simulation, we follow the same procedure as above except that the simulated bleaching anisotropy contains no fast component while retaining the initial value of 0.1. This is accomplished by setting $k_1 = 0$ and $k_3 = 0.05$ with all other parameters the same as in Eq. A1. The result returned by the fitting procedure is a highly uncertain fast component rate $D_1 = 8{,}100 \pm 17{,}800\ s^{-1}$ with a tiny amplitude fraction of $6 \pm 6\%$. The slow rate, on the other hand, is reported reasonably accurately with $D_2 = 570 \pm 70\ s^{-1}$ and a large amplitude fraction of $94 \pm 6\%$. We can conclude that our fitting procedure reports the existence and approximate rate of a fast component only if it really exists.

We thank Drs. Robert Fulbright, Cynthia Marcelo, and Ariane McKiernan for their technical advice and Dr. Kate Barald for many useful discussions on both the details and direction of this project. We also thank Sharada Kumar for technical support including preparation of the cell cultures.

This work was supported by National Institutes of Health grant NS14565 and National Science Foundation grant DMB8805296 and, in the last stages, by National Science Foundation grant MCB9405928.

REFERENCES

Anderson, M. J., and M. W. Cohen. 1977. Nerve-induced and spontaneous redistribution of acetylcholine receptors on cultured muscle cells. *J. Physiol.* 268:757–773.

Axelrod, D. 1989. Fluorescence polarization microscopy. *Methods Cell Biol.* 30:333–352.

Axelrod, D., P. M. Ravdin, D. E. Koppel, J. Schlessinger, W. W. Webb, E. L. Elson, and T. R. Podleski. 1976. Lateral motion of fluorescently labeled acetylcholine receptor in membranes of developing muscle fibers. *Proc. Natl. Acad. Sci. USA.* 73:4594–4598.

Axelrod, D, P. M. Ravdin, and T. R. Podleski. 1978. Control of acetylcholine receptor mobility and distribution in cultured muscle membrane. *Biochim. Biophy. Acta.* 511:23–38.

Axelrod, D., J. Rubenstein, Y. Yuan. 1992. Fast rotational diffusion measured by fluorescence recovery after photobleaching. *Am. Chem. Polymer. Prep.* 33:755–756.

Barald, K. F., G. D. Phillips, J. C. Jay, and I. F. Mizukami. 1987. A component in mammalian muscle synaptic basal lamina induces clustering of aceylcholine receptors. *Prog. Brain Res.* 71:397–407.

Bartholdi, M., F. J. Barrantes, and T. M. Jovin. 1981. Rotational molecular dynamics of the membrane-bound acetylcholine receptor revealed by phosphorescence spectroscopy. *Eur. J. Biochem.* 120:389–397.

Bevington, P. R., and D. K. Robinson. 1992. *Data Reduction and Error Analysis for the Physical Sciences,* 2nd ed. McGraw-Hill, New York.

Bloch, R. J., M. Velez, J. G. Krikorian, and D. Axelrod. 1989. Microfilaments and actin-associated proteins at sites of membrane-substrate attachment within acetylcholine receptor clusters. *Exp. Cell Res.* 182: 583–596.

Bradford, M. M. 1976. A rapid and sensitive method for the quantitation of microgram quantities of protein utilizing the principle of protein-dye binding. *Anal. Biochem.* 72:248–254.

Brisson, A., and P. N. Unwin. 1985. Quaternary structure of the acetylcholine receptor. *Nature.* 315:474–477.

Campanelli, J. T., W. Hoch, F. Rupp, T. Kreiner, and R. H. Scheller. 1991. Agrin mediates cell contact induced acetylcholine receptor clustering. *Cell.* 67:909–916.

Cherry, R. J. 1979. Rotational and lateral diffusion of membrane proteins. *Biochim. Biophys. Acta.* 559:289–327.

Daniels, M. P. 1990. Localization of actin, β-spectrin, 43×10^3 M_r and 58×10^3 M_r proteins to receptor-enriched domains of newly formed acetylcholine receptor aggregates in isolated myotube membranes. *J. Cell Sci.* 97:615–627.

Daniels, M. P., J. G. Krikorian, A. J. Olek, and R. J. Bloch. 1990. Association of cytoskeletal proteins with newly formed acetylcholine receptor aggregation induced by embryonic brain extract. *Exp. Cell Res.* 186:99–108.

Edidin, M. 1987. Rotational and lateral diffusion of membrane proteins and lipids: phenomena and function. *Curr. Topics Membr. Transp.* 29: 91–127.

Falls, D. L., D. A. Harris, F. A. Johnson, M. M. Morgan, G. Corfas, and G. D. Fischbach. 1990. Mr 42,000 ARIA: a protein that many regulate the accumulation of acetylcholine receptors at developing chick neuromuscular junctions. *Cold Spring Harb. Symp. Quant. Biol.* 55:397–406.

Frank, E., and G. D. Fischbach. 1979. Early events in neuromuscular junction formation in vitro. *J. Cell Biol.* 83:143–158.

Fulbright, R. F., and D. Axelrod. 1993. Dynamics of nonspecific adsorption of insulin to erythrocyte membranes. *J. Fluor.* 3:1–16.

Godfrey, E. W., R. M. Nitkin, B. G. Wallace, L. L. Rubin, and U. J. McMahan. 1984. Components of *Torpedo* electric organ and muscle that cause aggregation of acetylcholine receptors on cultured muscle cells. *J. Cell Biol.* 99:615–627.

Hellen, E. H., K. Ajtai, and T. P. Burghardt. 1993. Myosin head rotation in muscle fibers measured using polarized fluorescence photobleaching recovery. *Biophys. J.* 64:A28.

Hellen, E. H., and T. P. Burghardt. 1994. Saturation effects in polarized fluorescence photobleaching recovery and steady state fluorescence polarization. *Biophys. J.* 66:1–7.

Jacobson, B. S., J. Cronin, and D. Branton. 1978. Coupling polylysine to glass beads for plasma membrane isolation. *Biochim. Biophys. Acta.* 506:81–96.

Jessell, T. M., R. E. Siegel, and G. D. Fischbach. 1979. Induction of acetylcholine receptors on cultured skeletal muscle by a factor extracted from brain and spinal cord. *Proc. Natl. Acad. Sci. USA.* 76:5397–5401.

Knaack, D., T. R. Podleski, and M. M. Salpeter. 1987. Ascorbic acid and acetylcholine receptor expression. *Ann. NY Acad. Sci.* 498:77–89.

Lo, M., P. Garland, J. Lamprecht, and E. Barnard. 1980. Rotational mobility of the membrane-bound acetylcholine receptor of *Torpedo* electric organ measured by phosphorescence depolarization. *FEBS Lett.* 111:407–412.

Lupa, M. T., and J. H. Caldwell. 1991. Effect of agrin on the distribution of acetylcholine receptors and sodium channels on adult skeletal muscle fibers in culture. *J. Cell Biol.* 115:765–778.

Nastuk, M. A., and J. R. Fallon. 1993. Agrin and the molecular choreography of synapse formation. *Trends Neurosci.* 16:72–76.

Neugebauer, K., M. M. Salpeter, and T. R. Podleski. 1985. Differential responses of L5 and rat primary muscle cells to factors in rat brain extract. *Brain Res.* 346:58–69.

Olek, A. J., P. A. Pudimat, and M. P. Daniels. 1983. Direct observation of the rapid aggregation of acetylcholine receptors on identified cultured myotubes after exposure to embryonic brain extract. *Cell.* 34:255–264.

Peng, H. B., P-C. Cheng, and P. W. Luther. 1981. Formation of ACh receptor clusters induced by positively charged latex beads. *Nature.* 292:831–834.

Podleski, T. R., D. Axelrod, P. Ravdin, I. Greenberg, M. M. Johnson, and M. N. Salpeter. 1978. Nerve extract induces increase and redistribution of acetylcholine receptors on cloned muscle cells. *Proc. Natl. Acad. Sci. USA.* 75:2035–2039.

Poo, M., and S. Young. 1990. Diffusional and electrokinetic redistribution at the synapse: a physicochemical basis of synaptic competition. *J. Neurobiol.* 21:157–168.

Rahman, N. A., I. Pecht, D. A. Roess, and B. G. Barisas. 1992. Rotational dynamics of type I Fc epsilon receptors on individually-selected rat mast cells studied by polarized fluorescence depletion. *Biophys. J.* 61:334–346.

Reist, N. E., M. J. Werle, and U. J. McMahan. 1992. Agrin released by motor neurons induce the aggregation of acetylcholine receptors at neuromuscular junctions. *Neuron.* 8:865–868.

Rochlin, M. W., and H. B. Peng. 1989. Localization of intracellular proteins at acetylcholine receptor clusters induced by electric fields in *Xenopus* muscle cells. *J. Cell Sci.* 94:73–83.

Rousselet, A., J. Cartaud, P. Devaux, and J-P. Changeux. 1982. The rotational diffusion of the acetylcholine receptor in *T. marmorata* membrane fragments studied with a spin-labeled α-toxin: importance of the 43k protein. *EMBO J.* 1:439–445.

Saffman, P. G., and M. Delbruck. 1975. Brownian motion in biological membranes. *Proc. Natl. Acad. Sci. USA.* 72:3111–3113.

Salpeter, M. M., S. Spanton, K. Holley, and T. R. Podleski. 1982. Brain extract causes acetylcholine receptor redistribution which mimics some early events at developing neuromuscular junctions. *J. Cell Biol.* 93: 417–425.

Scalettar, B., P. Selvin, D. Axelrod, J. Hearst, and M. P. Klein. 1990. A polarized photobleaching study of DNA reorientation in agarose gels. *Biochemistry.* 29:4790–4798.

Selvin, P. R., B. A. Scalettar, J. P. Langmore, D. Axelrod, M. P. Klein, and J. E. Hearst. 1990. A polarized photobleaching study of chromatin reorientation in intact nuclei. *J. Mol. Biol.* 214:911–922.

Shadiack, A. M., and A. M. Nitkin. 1991. Agrin induces α-actinin, filamin, and vinculin to co-localize with AChR clusters on cultured chick myotubes. *J. Neurobiol.* 22:617–628.

Stollberg, J., and S. E. Fraser. 1988. Acetylcholine receptors and concanavalin A-binding sites on cultured *Xenopus* muscle cells: electrophoresis, diffusion and aggregation. *J. Cell Biol.* 107:1397–1408.

Stollberg, J., and S. E. Fraser. 1990a. Local accumulation of acetylcholine receptors is neither necessary nor sufficient to induce cluster formation. *J. Neurosci.* 10:247–255.

Stollberg, J., and S. E. Fraser. 1990b. Acetylcholine receptor clustering is triggered by a change in the density of a nonreceptor molecule. *J. Cell Biol.* 111:2029–2039.

Stya, M., and D. Axelrod. 1983. Diffusely distributed acetylcholine receptors can participate in cluster formation on cultured rat myotubes. *Proc. Natl. Acad. Sci. USA.* 80:449–453.

Timbs, M. M., and N. L. Thompson. 1990. Slow rotational mobilities of antibodies and lipids associated with substrate supported phospholipid monolayers as measured by polarized fluorescence photobleaching recovery. *Biophys. J.* 58:413–428.

Velez, M., and D. Axelrod. 1988. Polarized fluorescence photobleaching recovery for measuring rotational diffusion in solutions and membranes. *Biophys. J.* 53:575–591.

Velez, M., K. F. Barald, and D. Axelrod. 1990. Rotational diffusion of acetylcholine receptors on cultured rat myotubes. *J. Cell Biol.* 110: 2049–2059.

Wallace, B. G. 1989. Agrin-induced specializations contain cytoplasmic, membrane, and extracellular matrix-associated components of the postsynaptic apparatus. *J. Neurosci.* 9:1294–1302.

Yoshida, T. M., and B. G. Barisas. 1986. Protein rotational motion in solution measured by polarized fluorescence depletion. *Biophys. J.* 50:41–53.

Yuan, Y. 1994. Polarized fluorescence photobleaching for measuring fast rotational motion of cell surface receptors. Ph.D. thesis. The University of Michigan, Ann Arbor, Michigan. 112 pp.

Yuan, Y., and D. Axelrod. 1994. Photobleaching with a subnanosecond laser flash. *J. Fluor.* 4:141–151.